AIMS Materials Science, 13(2): 282–299.
DOI: 10.3934/matersci.2026016
Received: 05 February 2026
Revised: 16 March 2026
Accepted: 20 March 2026
Published: 26 March 2026

https://www.aimspress.com/journal/Materials

Research article

Relative contribution of oxide bifilms and micro-voids to tensile property of Al-7Si-0.4Mg alloys

Choongdo Lee*

Department of Materials Science and Engineering, Inha Technical College, Michuhol-gu, Incheon, South Korea

Abstracts: This study aims to evaluate the relative contribution of shrinkage voids and oxide bifilms to the tensile properties of Al-7Si-0.4Mg alloys in terms of defect susceptibility due to the existence of casting defects. Tensile specimens were fabricated via gravity casting using commercial A356 aluminum alloy, and the area fraction of casting defects was measured using scanning electron microscope (SEM) fractographic analysis of the tensile fracture surfaces. Shrinkage voids and oxide bifilms are representative casting defects that significantly influence the tensile properties of A356 alloys. When oxide bifilms are present alongside shrinkage voids, tensile properties exhibit greater sensitivity to changes in the area fraction of casting defects compared to specimens containing only micro-voids in the form of shrinkage voids containing a thin oxide film. However, the defect susceptibility coefficients for tensile strength and elongation under T6-treated conditions are somewhat lower than those observed in the as-cast specimens. In this study, the area fraction of oxide bifilms on the fracture surfaces of the tensile specimens averaged 12.5%, with an inclusion frequency of approximately 45%, which is relatively lower than that of shrinkage voids present on all fracture surfaces. The defect susceptibility coefficients for tensile strength and elongation in as-cast specimens where the casting defects consisted solely of oxide bifilms were approximately 3.58 and 11.34, respectively. These values represent clear increases of approximately 3.2 and 9.1 compared to specimens containing only shrinkage voids; a similar trend was observed under T6-treated conditions.

Keywords: aluminum alloy; bifilm; shrinkage void; tensile property; defect susceptibility

1. Introduction

Casting materials are highly sensitive to melt quality, microstructure, and the presence of casting defects, all of which are influenced by the manufacturing process design. Representative defects in castings manufactured through conventional casting processes include shrinkage voids and blow holes formed in conjunction with gas release and volume change during the solid–liquid transformation process, as well as casting defects such as entrapped bubbles, bifilms, and foreign inclusions introduced during pouring, feeding, supply, or transport processes [1–3]. The formation process of these extrinsic defects is related to surface turbulence, laminar flow, and submergence of the charge material involved in the pouring, feeding, and transport processes accompanying the casting process of molten metal [1,4–6]. In particular, a representative extrinsic defect in aluminum alloys is the oxide bifilm, which plays a decisive role in reducing the load-carrying capacity per unit volume of the material through the formation of a thin oxide film formed by the oxygen affinity of aluminum [7–9]. Therefore, several works have been conducted to assess the dependence of mechanical properties on the presence of oxide bifilms and their formation mechanism [2,3,10–12].

As a representative study, Dispinar et al. reported that the content of oxide bifilms in cast aluminum alloys can be quantified using the bifilm index [4,5], which is closely related to changes in the concentration of hydrogen and oxygen in the melt and atmosphere. They systematically investigated the correlation between hydrogen concentration, mechanical properties, and pore number by measuring the bifilm index of test specimens manufactured through reduced pressure tests (RPT) targeting representative commercial aluminum alloys (A356, A319, and A380 alloys) [4,5]. Regarding the experimental approach using the RPT test, Tiryakioğlu et al. confirmed the presence of a thin oxide film in the dendritic solidification zone around the shrinkage void through scanning electron microscope (SEM) and energy dispersive X-ray spectrometry (EDS) analysis of the A356 alloy [8]. In addition, Eisaabadi et al. and Bogdanoff et al. reported through systematic experiments that the dependence of tensile and fatigue properties on the presence of oxide bifilms is more sensitive than the presence of micro-voids [2,3,9].

Recently, Liu et al. reported that hydrogen adsorbed during the bifilm formation process can affect interfacial separation, which significantly reduces mechanical properties [13]. In addition, Kavousi et al. investigated the wetting characteristics of nanostructures and the formation and growth of oxide in molten aluminum using molecular dynamics simulation [14].

However, complete elimination of oxide inclusions and micro-voids as structural defects is extremely challenging in practice [1–3]. The presence of such structural defects critically affects the mechanical properties of components, influencing both the effective load-carrying capacity and the mechanisms of crack growth and coalescence [15–17]. Consequently, significant research has focused on the formation of micro-voids—a representative intrinsic casting defect—and their impact on mechanical properties.

The concept of defect susceptibility, proposed by Gokhale et al., provides a quantitative framework for describing the influence of micro-voids on tensile properties of aluminum alloy castings [15,16]. The dependence of tensile elongation on changes in micro-porosity of A356 aluminum alloy can be expressed in terms of a defect susceptibility coefficient and the maximum elongation achievable under void-free conditions, as shown in Eq 1 [15,16]:

$$e = e_0[1 - f]^a \tag{1}$$

here, e represents the elongation corresponding to a microporosity f, while e_o and a denote the maximum elongation and the defect susceptibility coefficient achievable under defect-free conditions, respectively. This relationship, as expressed in Eq 2, has also been shown to be applicable to tensile strength in subsequent studies on various alloy conditions [18,19].

$$S = S_0[1 - f]^b \tag{2}$$

Similarly, S and S_o represent the tensile strength corresponding to a microporosity f and the maximum tensile strength achievable under microporosity-free conditions, respectively, while b denotes the defect susceptibility coefficient of tensile strength with respect to changes in microporosity.

Despite ongoing research on the effects of casting defects on the tensile properties of cast materials, only a few studies have quantitatively analyzed the degradation of mechanical properties caused by oxide bifilms, a representative extrinsic defect in aluminum alloys [2,3].

In this study, the dependence of tensile properties on the presence of micro-voids and oxide bifilms—two representative casting defects in A356 alloy—was investigated. Furthermore, the relative contributions of these defects to the degradation of tensile properties were quantitatively assessed from the perspective of defect susceptibility.

2. Materials and methods

2.1. Materials and specimen preparation

Specimens in this study were manufactured using gravity casting with commercial A356 alloy. Melting was performed in an electric resistance furnace under an atmosphere using a high-purity graphite crucible with an inner diameter of 110 mm, containing 1.8 kg of virgin ingot. The molten metal was maintained at 700 °C after skimming and drossing and then poured into a multistep metallic mold by the gravity-casting method. A schematic diagram of a multistep metallic mold (plain carbon steel) is shown in Figure 1. As shown, the mold had a multistep geometry with a width of 120 mm, a height of 100 mm, and cavity thicknesses of 8, 16, and 24 mm, and was maintained at 250 °C using an electric heating element.

In addition, the surface inside the mold was coated with boron nitride powder to ensure smooth extraction after casting, along with uniform heat transfer to the mold. Specimens for microstructural observation and tensile testing were taken from the mold section with a thickness of 16 mm and were produced under both as-cast and T6-treated conditions (solutionizing at 540 °C for 6 h, followed by artificial aging at 180 °C for 18 h).

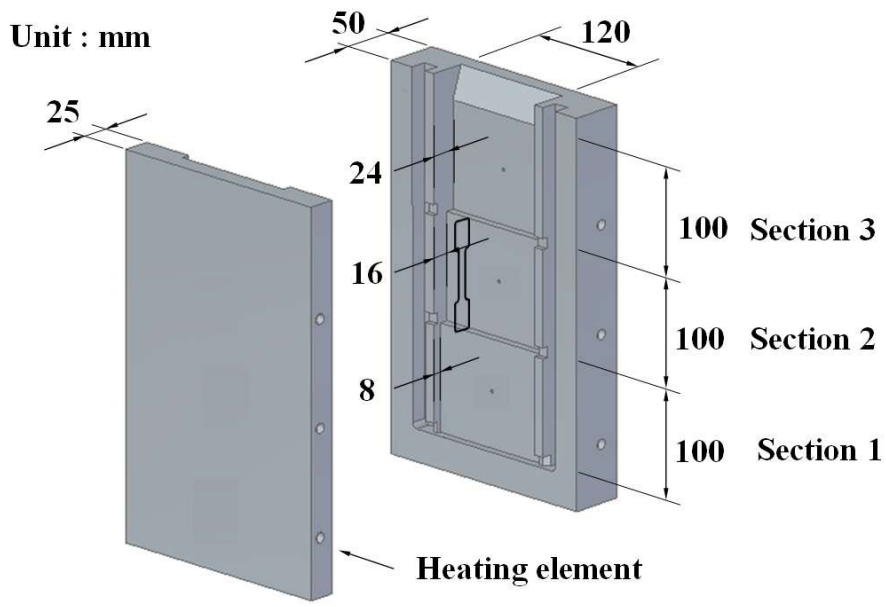

Figure 1. Schematic diagram of the multistep metallic mold for the fabrication of the test specimen.

2.2. Chemical analysis and microstructural observation

The chemical composition of the specimens was analyzed using optical emission spectrometry (OES; Bruker Q4-TASMAN), and the results are summarized in Table 1. Microstructural observations, including the identification of casting defects, were conducted using an optical microscope. Specimens were polished and subsequently etched by immersion in a 2% hydrofluoric acid (HF) aqueous solution for approximately 10 s. The microstructural characteristics, such as grain size and secondary dendrite arm spacing (SDAS) of the as-cast condition, were measured using the line intercept method. To investigate the crack propagation path during tensile deformation, the microstructure was examined in the cross-sectional direction perpendicular to the tensile fracture surface, with particular focus on regions containing casting defects.

Table 1. Chemical composition of A356 aluminum alloy.

Elements	Composition (wt.%)
Si	7.17
Cu	0.02
Mg	0.45
Fe	0.02
Mn	0.01
Ti	0.124
Sr	0.002
Al	Bal.

2.3. Tensile test and microporosity measurement

Tensile specimens were fabricated as a plate type with a gauge length of 30 mm and a gauge width of 6 mm. The thickness of the test pieces ranged from approximately 1.1 to 2.0 mm, and 25 pieces were manufactured for each as-cast and T6-treated condition. Tensile tests were conducted at room temperature using a universal testing machine (UTM; Instron 5985) equipped with an extensometer, at a strain rate of 6.56×10^{-4} s^{-1}. The area fraction of casting defects was determined by comparing the total area of defects measured via scanning electron microscopy (SEM; JEOL JSM5600) observation to the overall fracture surface area of each tensile specimen. In this study, casting defects were broadly classified into micro-voids and oxide bifilms, and the total area fraction of these defects was measured by comparing the sum of the individual areas of each defect to the entire area of the tensile fracture surface. The individual area of micro-voids was measured only by selecting the void region in the shape of a shrinkage void with a dendritic growth pattern. The oxide bifilm was measured for the region with the shape of a thin oxide film formed by the interfacial separation between oxide layers or between the oxide and the matrix region; this was confirmed as a fracture region of a similar shape based on the results of EDS analysis (JEOL Oxford X-max). EDS analysis was performed at an input rate of at least 300 kcps through automatic process time setting with automatic ZAF correction under non-standard sample method conditions, which are common EDS analysis conditions, at an acceleration voltage of 20 kV, the acceleration voltage for SEM observation.

3. Results

3.1. Microstructural characteristics

The microstructural characteristics of the test specimens produced in this study had a typical cast structure of an A356 alloy; the average grain size and SDAS were measured as 204.1 and 46.3 μm, respectively, based on the as-cast condition. Figure 2 shows the optical micrographs of the distribution patterns of micro-voids and oxide biofilms observed by optical microscope (OM), which are representative entrainment defects present in T6-treated A356 alloy, along with SEM images of locally present casting defects and EDS mapping results for oxygen elements. In Figure 2a, micro-voids and oxide bifilms are seen coexisting locally within the typical A356 microstructure composed of primary Al and eutectic Si particles. As shown in Figure 2a, micro-voids are primarily distributed singly or in clusters near eutectic Si particles, forming shrinkage voids. These shrinkage-type micro-voids are typical entrainment defects that are mixed into Al alloy castings along with oxide bifilms and are characterized by the formation of a thin oxide film on the surface of dendritic-shaped solid particles existing inside the micro-voids [1–3,5,8]. The formation and inclusion of oxides in micropore formation could also be observed in this study. As shown in the EDS mapping results for oxygen elements in Figure 2b,c, traces of oxide formation accompanying the solidification process can be observed on the surface of the dendritic region existing inside the shrinkage void. In contrast, Figure 2d shows oxide bifilms as thin, irregular linear features present throughout both eutectic and primary Al regions. Even in the case of such a thin oxide bifilm, the formation and inclusion of oxides can be clearly observed, as shown in the EDS mapping results for oxygen elements in Figure 2e,f.

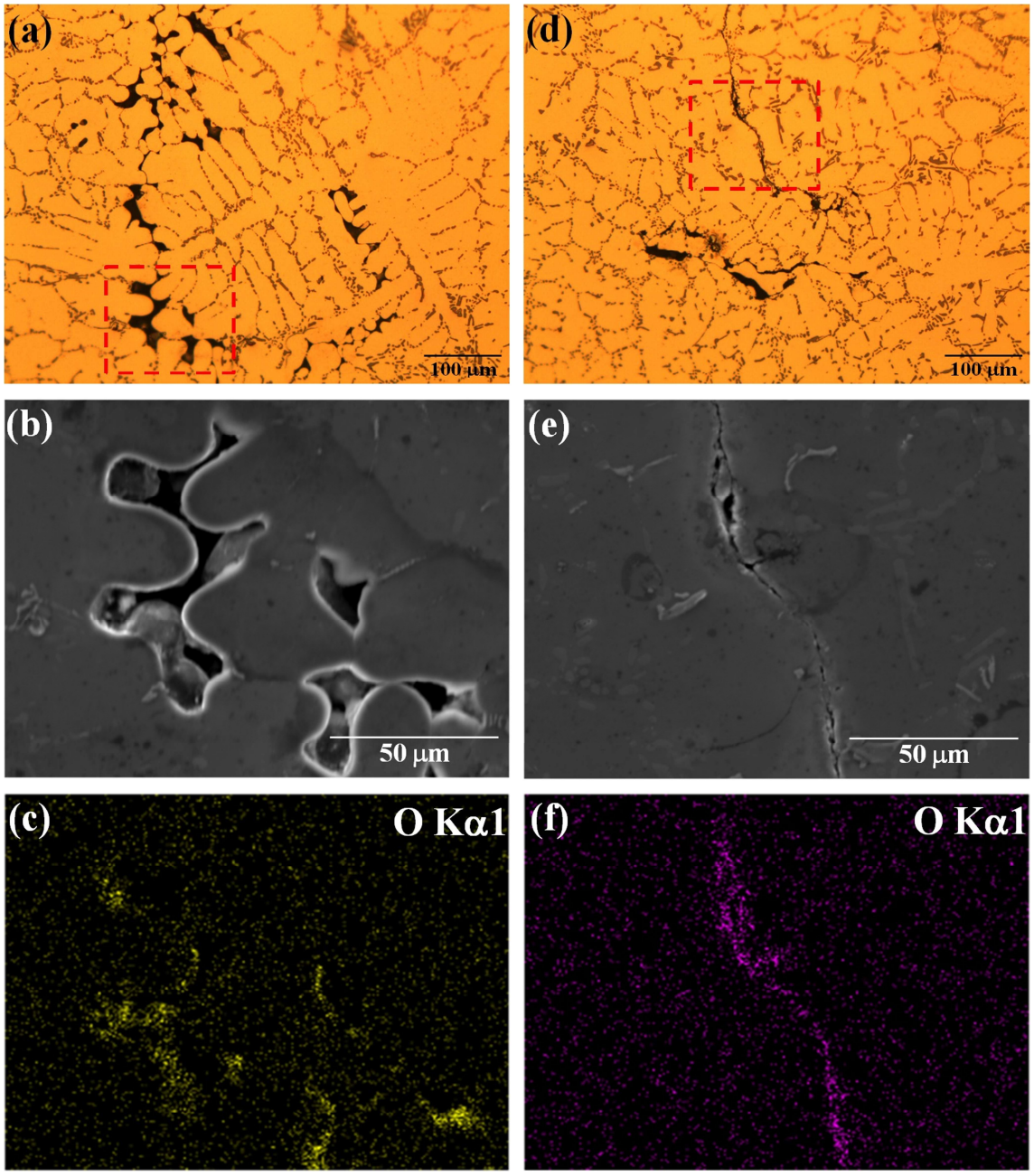

Figure 2. Optical microscope images of micropores and oxide bifilms present in A356 alloy, SEM images of local regions, and EDS mapping results for oxygen elements: (a–c) OM and SEM/EDS mapped images of micro-voids, (d–f) OM and SEM/EDS mapped images of oxide bifilms.

3.2. Tensile properties and fractographic analysis

The nominal values of tensile properties measured in this study are summarized in Table 2. For as-cast specimens, the average values of yield strength (YS) and ultimate tensile strength (UTS) were approximately 115 and 172 MPa, respectively, with an elongation of 2.1%. For T6-treated specimens, the yield and tensile strengths increased to 264 and 282 MPa, respectively, while elongation decreased to 0.7%, indicating a significant effect of T6 treatment on mechanical performance. In any case, as

summarized in Table 2, the tensile properties of the T6 treatment condition show a significant increase in yield strength and tensile strength compared to the as-prepared condition, but a relatively low level of elongation. This is because the artificial aging treatment condition of 180 °C/18 h in this study corresponds to peak aging in terms of strength but to the end of peak aging in terms of elongation [18]. In any case, even under the uniform manufacturing process and microstructural conditions, the tensile properties show a considerable deviation in both the as-cast and T6-treated conditions. Despite uniform manufacturing and microstructural characteristics, large deviations in tensile properties were observed under both conditions. Fractographic analysis using SEM revealed that these deviations were primarily caused by the presence of casting defects.

Table 2. Tensile properties of the A356 alloy in as-cast and T6-treated conditions.

Alloy condition	Yield strength (MPa) (+/–)	Ultimate tensile strength (MPa) (+/–)	Elongation (%) (+/–)
As-cast condition	115.0 (+17.0/–14.6)	171.8 (+46.8/–69.0)	2.08 (+2.55/–1.62)
T6-treated condition	264.1 (+24.2/–58.8)	281.7 (+47.1/–74.9)	0.67 (+1.5/–0.46)

Figure 3 shows SEM observations of tensile fracture surfaces under as-cast and T6-treated conditions. Casting defects in the form of shrinkage voids mixed/formed in Al alloy castings contain a very thin oxide film locally [8]; in this study, the shapes of casting defects were largely divided into shrinkage void-shaped micro-voids containing a thin oxide film and oxide bifilms composed of a relatively thick oxide film: specimens containing only micro-voids (Figure 3a,b) and specimens containing both micro-voids and oxide bifilms (Figure 3c,d). Compared to cross-sectional microstructural observations (Figure 2), the fracture surfaces exhibit a much higher defect density. This is because the fracture surface corresponds to regions of the lowest load-carrying capacity, where tensile cracks preferentially initiate, propagate, and coalesce, i.e., regions with the highest effective void area fraction [17–19].

Figure 4 shows magnified views of defects on the fracture surfaces. As shown in Figure 3, the distribution patterns and areas of shrinkage voids and oxide bifilms observed in the SEM fractographic analysis can be clearly distinguished. Micro-voids (Figure 4a) display typical shrinkage void morphology with a dendritic solidification pattern. In contrast, oxide bifilms (Figure 4b) appear as broad, intercalated regions rather than the thin, irregular linear features observed in cross-sections (Figure 2c). This broad distribution arises because interfacial separation of the bifilm layers occurs readily under tensile loading, allowing the bifilm to unfurl and propagate over a wider area during crack growth. In any case, the area fraction of casting defects measured through SEM fractographic analysis is based on the area projected perpendicular to the tensile fracture surface. Therefore, there are clear limitations in accurately reflecting the load-carrying capacity of the actual tensile fracture surface, and this is expected to result in a certain level of measurement error.

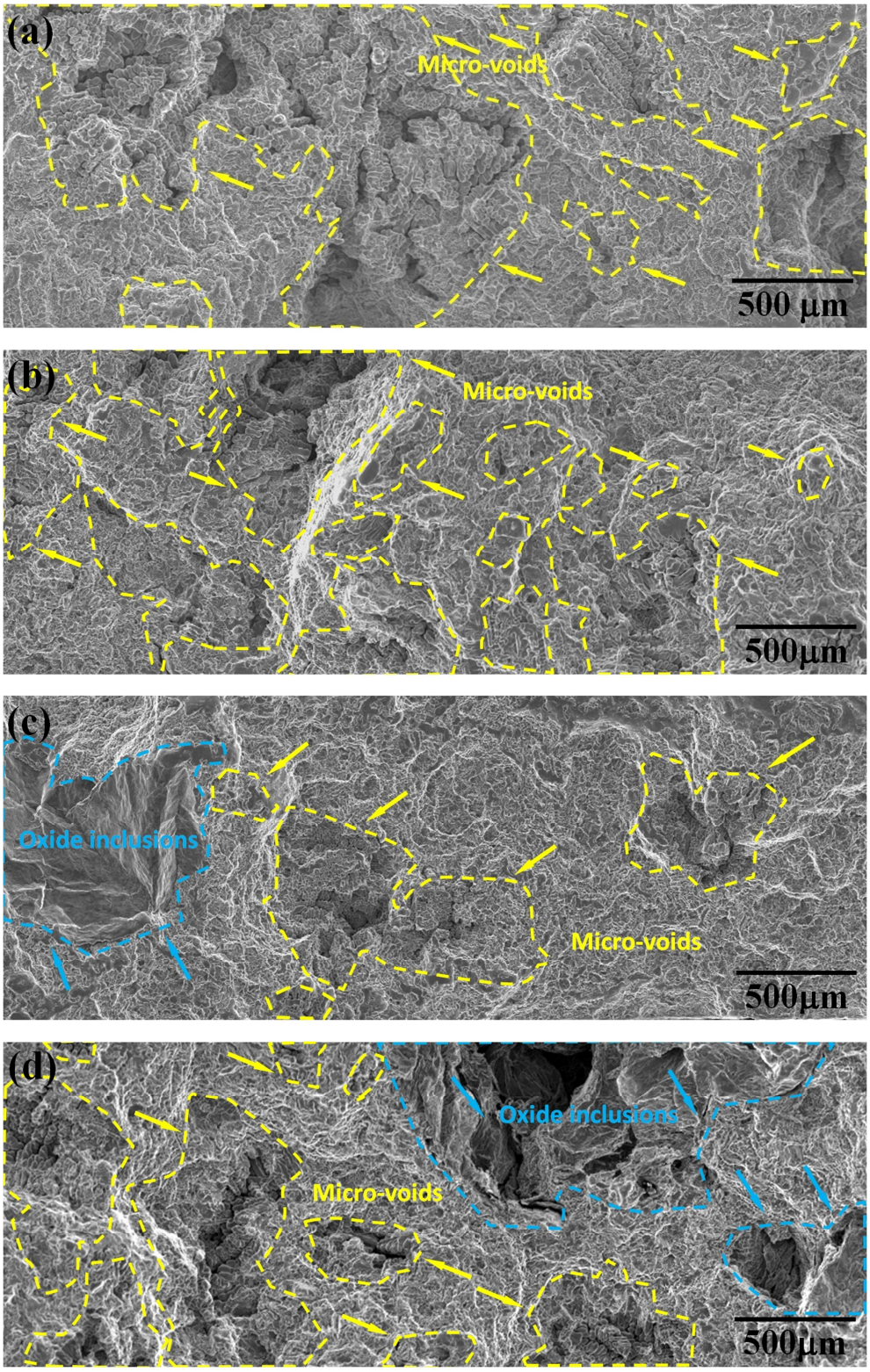

Figure 3. SEM images of tensile fracture surfaces of A356 alloy: (a, c) as-cast and (b, d) T6-treated conditions. (a, b) Specimens with only micro-voids; (c, d) specimens with both micro-voids and oxide bifilms.

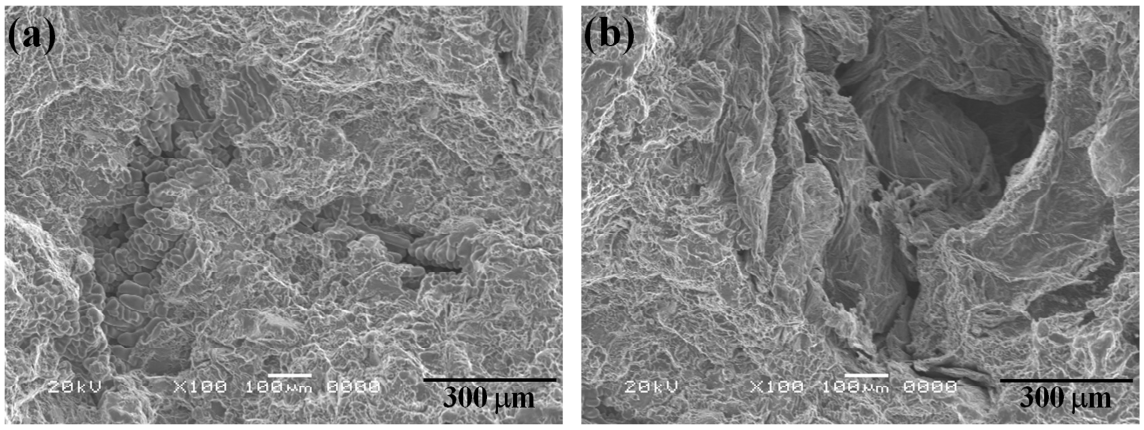

Figure 4. SEM images of casting defects on the fracture surface: (a) micro-voids, (b) oxide bifilms.

Table 3 summarizes the inclusion frequency and area fraction of shrinkage voids and oxide bifilms observed on the tensile fracture surfaces of all specimens, as determined by SEM fractographic analysis. The average inclusion frequency and area fraction of oxide bifilms under as-cast and T6-treated conditions were 44.4% and 11.5%, and 50.0% and 13.3%, respectively, indicating similar levels regardless of heat treatment. Shrinkage voids were observed in nearly all specimens, even at trace levels, while the inclusion frequency of oxide bifilms was approximately half, averaging 44.9%. The average area fraction of oxide bifilms was 12.5%, which corresponds to approximately 1/3 of the area fraction of all casting defects. The inclusion frequency and amount of oxide bifilms, like shrinkage voids, depend on the hydrogen content of the aluminum alloy melt, and can be improved by controlling the hydrogen content through melting atmosphere control and degassing treatments such as gas bubbling filtration/floatation (GBF) [3,5,7,20]. However, it has been recently reported that changes in the frequency and amount of bifilm formation due to melt flow during melt transport or mold filling can diminish the effectiveness of hydrogen content control [21,22].

Table 3. Frequency and area fraction of oxide bifilms in tensile fracture surfaces of A356 alloy.

Item	Alloy condition		
	As-cast	T6-treated	Average
Total number of specimens	25	24	-
Number and frequency of specimens containing oxide bifilms	10 (44.4%)	12 (50.0%)	- (44.9%)
Average area fraction of oxide bifilms (%) (+/–)	11.5 (7.6/5.1)	13.3 (14.9/9.9)	12.5 (15.6/9.1)
Total area fraction (bifilm + shrinkage) (%) (+/–)	29.7 (26.2/20.7)	36.2 (25.4/32.5)	32.9 (28.7/29.2)

Figure 5 shows the dependence of tensile properties on the total area fraction of casting defects (shrinkage voids plus oxide bifilms) on the fracture surface. The yield strength in the as-cast condition remained nearly constant at ~115 MPa, whereas in the T6-treated condition, it decreased slightly from ~290 to 250 MPa as the defect fraction increased to ~60% (Figure 5a). The elongation (0.2%) corresponding to the yield strength strictly corresponds to the elasto-plastic transition region, and in this region, the effective load-carrying capacity within the material to the overall level of the yield strength has a relatively lower contribution than the tensile strength or elongation. Moreover, in the as-cast condition, the elasto-plastic deformation behavior centered on the

pro-eutectic Al matrix region occurs under lower stress conditions than in the T6 treatment condition, so the contribution to the effective load-carrying capacity due to the presence of casting defects is further reduced.

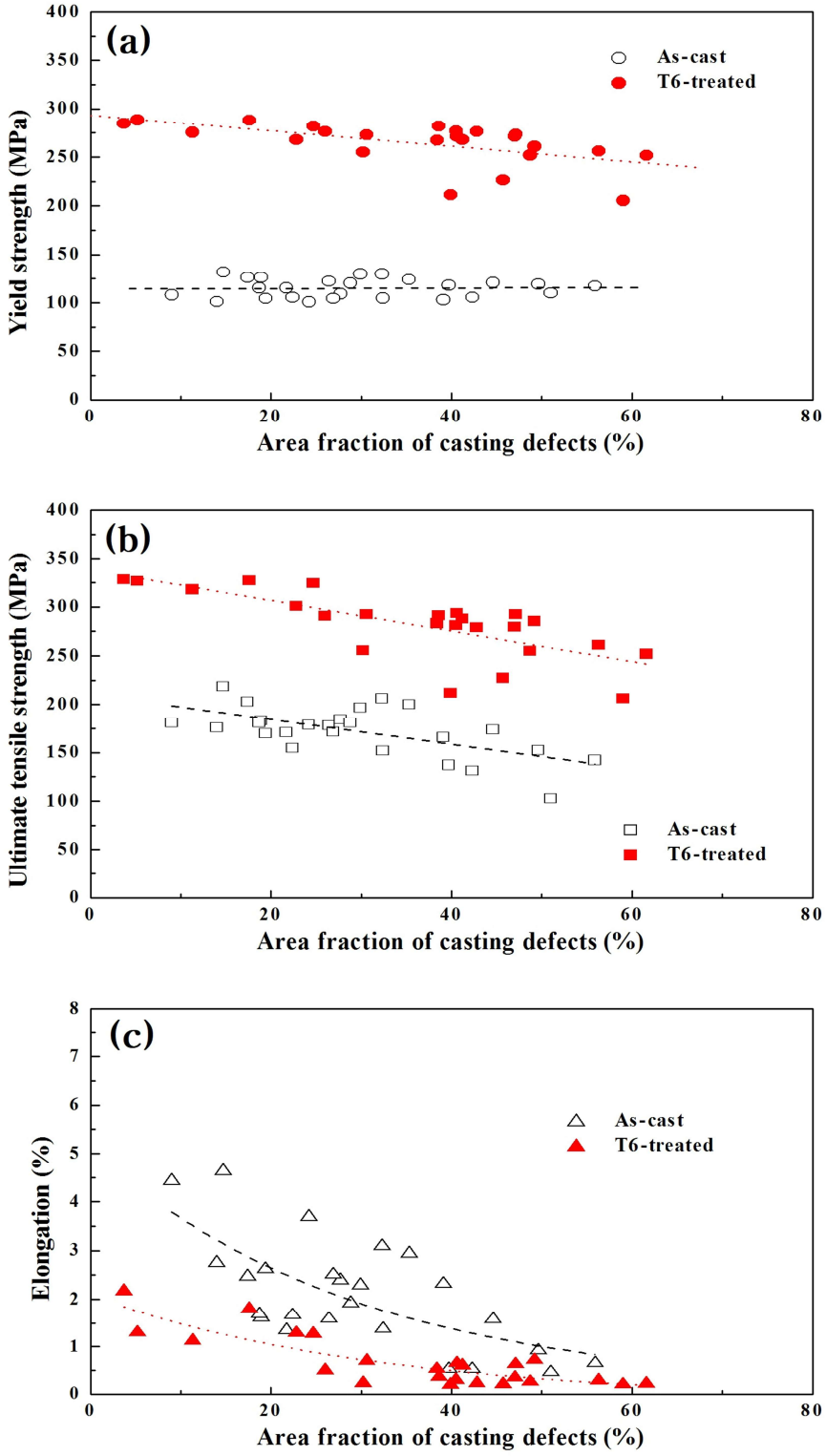

Figure 5. Dependence of tensile properties on the area fraction of casting defects present on the fracture surface: (a) yield strength; (b) ultimate tensile strength; and (c) elongation.

In contrast, ultimate tensile strength and elongation decreased markedly with increasing defect fraction in both conditions (Figure 5b,c). For example, in the T6-treated condition, tensile strength and elongation decreased from averages of 330 MPa and 2.0% to 250 MPa and 0.25%, respectively. This reduction is attributed to decreased effective load-carrying capacity and accelerated crack growth caused by stress concentrations around casting defects. Therefore, the observed deviations from the average values in Table 3 can be mainly attributed to variations in the area fraction of casting defects present on each fracture surface.

4. Discussions

4.1. Oxide bifilms

In Figure 2, SEM/EDS mapping results of micro-voids and oxide bifilms in local regions of the casting structure confirmed the formation and inclusion of oxides regardless of the type of defect. Although the inclusion of oxide layers in the formation process of entrainment defects has already been reported in several previous studies [1–3,8], EDS analysis was performed on casting defects present on the tensile fracture surface to clarify this. Figure 6 shows the SEM observation results and EDS analysis results for the oxide bifilm and shrinkage-shaped micro-voids present on the fracture surface. As shown in Figure 6a, the fracture morphology of the oxide bifilm region is distinctly different from that of the surrounding matrix, with small shrinkage voids observed in adjacent areas (right side of region A). EDS analysis (Figure 6b) detected the primary alloying elements Al, Si, and Mg, along with minor impurity elements such as Fe and Cu. The elemental concentrations exhibited slight variations across regions. Notably, the oxygen content in the normal fracture area (A) was approximately 2 wt.%, whereas the oxide bifilm region contained a significantly higher oxygen content of 35–39 wt.%, confirming that this region is composed predominantly of oxides. In addition, the oxygen content in the fracture region around the shrinkage voids shown in Figure 6c,d is 1.0–1.9 wt%, which is similar to that in Figure 6a, but the oxygen content in the shrinkage voids is 10–16 wt%. Although this is lower than the oxygen content of the oxide bifilm, it indirectly suggests that the shrinkage cavity with a dendritic growth pattern also undergoes the formation of an oxide film due to exposure to entrapped air during the bifilm formation and growth process [1–3].

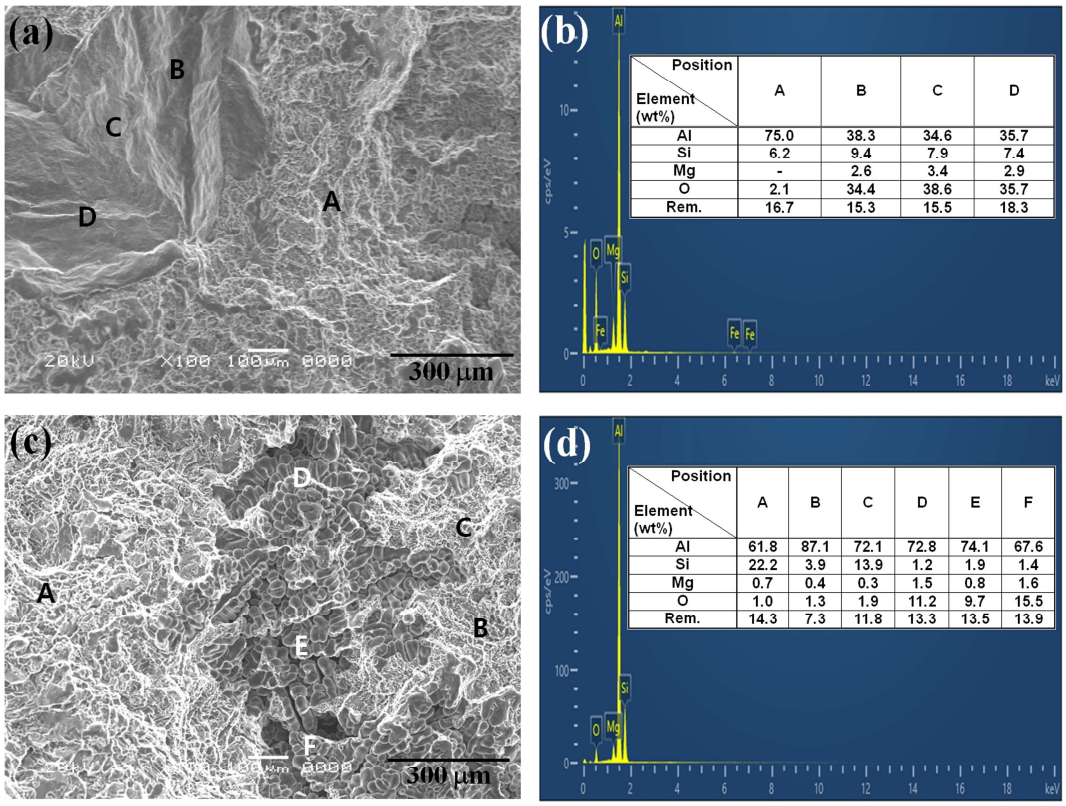

Figure 6. Representative results of SEM observation and EDS analysis for oxide bifilms and shrinkage voids present on the tensile fracture surface of a T6-treated specimen: (a, b) oxide bifilms and (c, d) shrinkage voids.

Figure 7 presents SEM and cross-sectional images of the oxide bifilm region on the fracture surface, with the fracture morphology of normal solidified microstructure. The microstructure of the circled region in Figure 7a shows that cracks propagated preferentially along the oxide film layers between the primary Al matrix and the eutectic Si-containing normally solidified structure. Adjacent oxide bifilms not directly on the main path of crack propagation also exhibited partial interfacial separation (Figure 7b).

This is distinct from the normally solidified regions, where crack growth is dominated by the early fracture of adjacent eutectic Si particles (Figure 7c). In essence, in Al–Si alloys containing micro-voids, tensile deformation is characterized by crack growth initiating at micro-voids and subsequently causing premature fracture of nearby Si particles [17–19]. In contrast, in regions containing oxide bifilms, crack growth is governed by the low load-carrying capacity of the oxide inclusion itself, leading to interfacial delamination and propagation along the oxide layer without significantly affecting surrounding eutectic Si particles or other defects. This is consistent with the results of a study conducted by Kutsal et al. that showed that the intra-structural arrangement of oxide bifilms significantly affects the overall fracture pattern and mechanical properties of aluminum castings [11].

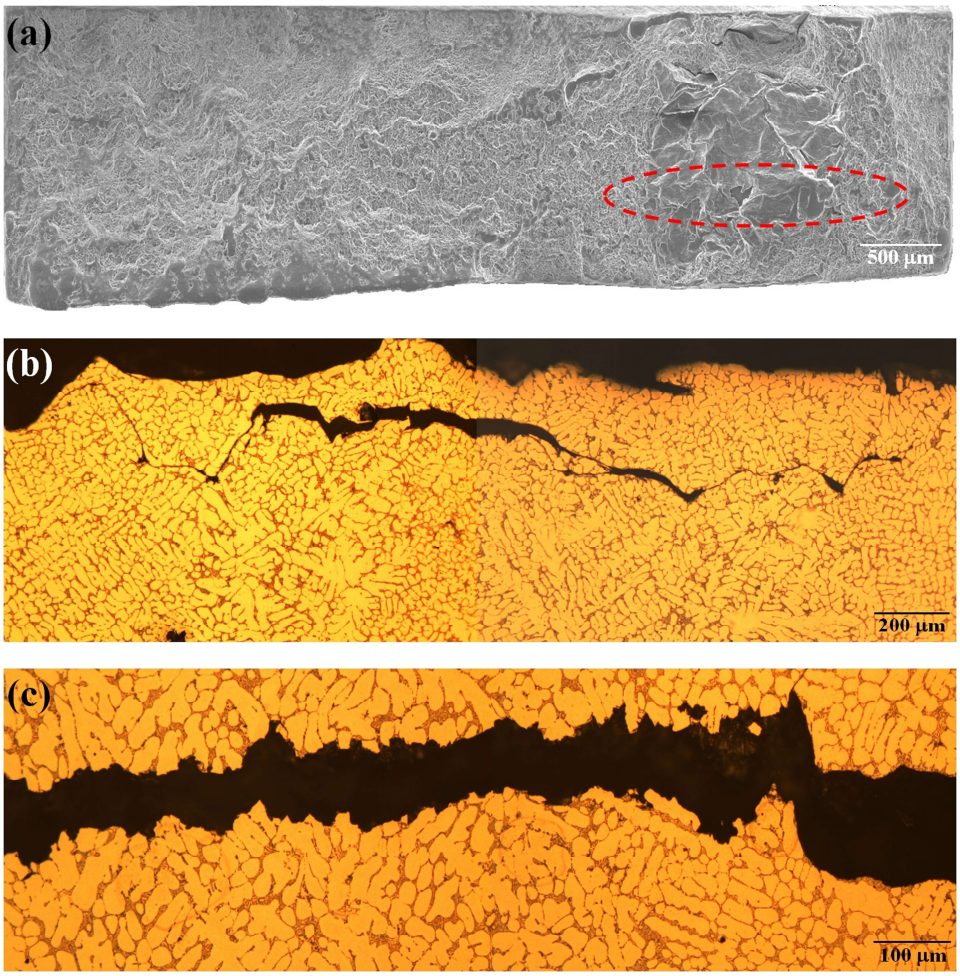

Figure 7. SEM image of oxide bifilms present on the tensile fracture surface and cross-sectional images of the corresponding region showing crack propagation along the oxide film layers.

4.2. Oxide bifilms vs. shrinkage voids on tensile properties

Oxide bifilms are casting defects that contribute more significantly to the degradation of tensile properties than shrinkage voids, as they shorten the crack propagation path during tensile deformation [4,5]. This effect was confirmed in this study through the cross-sectional observations of oxide bifilms on the fracture surface (Figure 7). Accordingly, the dependence of tensile strength and elongation on the total area fraction of casting defects (Figure 5) can vary according to the defect type.

Figure 8 shows the relationship between tensile properties and the area fractions of shrinkage voids and oxide bifilms in the as-cast and T6-treated conditions. In the legend of the figure, [bifilm + shrinkage] and [shrinkage void, only] refer to the specimen with coexistence of two types of casting defects and the specimen with only micro-voids in the form of shrinkage voids, respectively; [oxide bifilm, only] indicates only the area fraction of oxide bifilm in a specimen with two types of casting defects coexisting. In addition, Table 4 summarizes the defect susceptibility coefficients and the maximum values achievable under defect-free conditions (f = 0) for each defect condition. The dependence of tensile strength and elongation on the area fraction of casting defects can be described linearly, consistent with Eqs 1 and 2. Notably, the slope of the defect susceptibility coefficient for

specimens containing only shrinkage voids is lower than that for specimens containing both shrinkage voids and oxide bifilms, regardless of T6-treatment. Although the area fraction of oxide bifilms is relatively small compared to shrinkage voids, its influence on tensile properties is disproportionately high. Furthermore, the maximum achievable tensile properties under defect-free conditions are also affected by the presence of oxide bifilms.

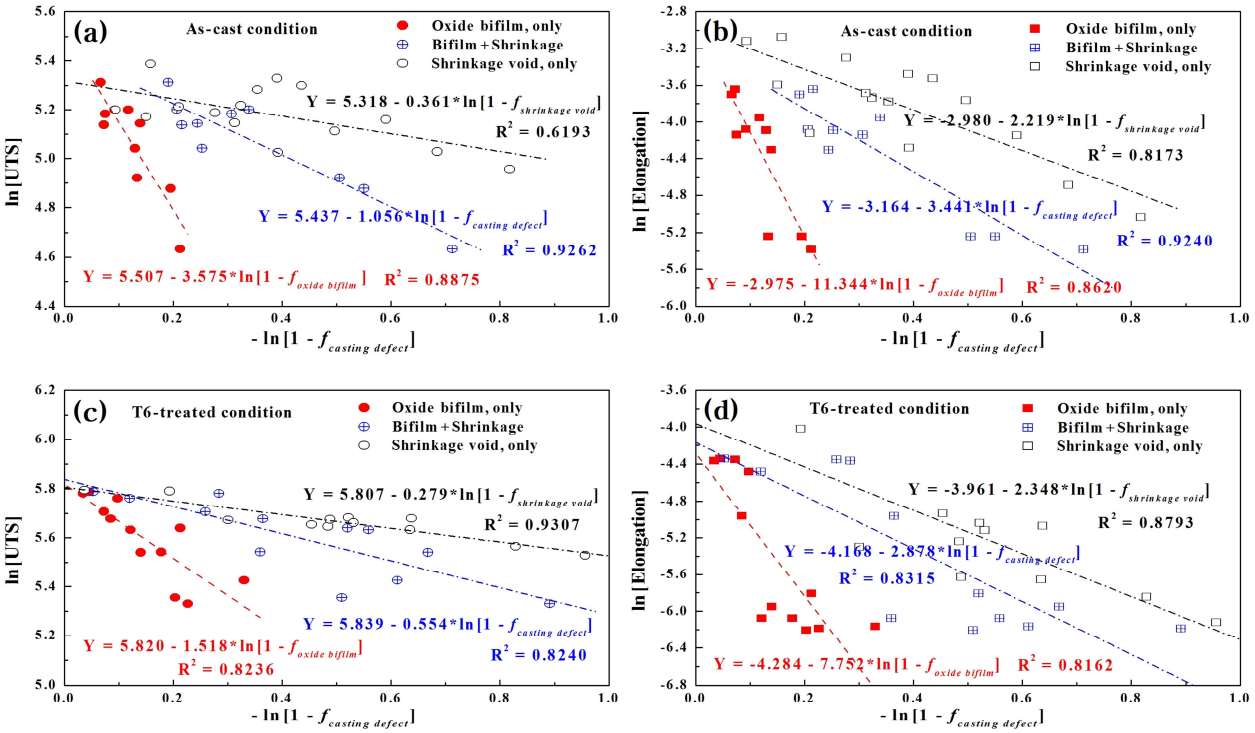

Figure 8. Defect susceptibility of (a, c) ultimate tensile strength and (b, d) elongation to the type and area fraction of casting defects. (a, b) As-cast and (c, d) T6-treated conditions.

Table 4. Defect susceptibility coefficients for tensile strength and elongation according to casting defect type and the maximum values achievable under defect-free conditions.

Alloy condition	Defects	Ultimate tensile strength		Elongation	
		Defect susceptibility coefficient	Max. value (MPa)	Defect susceptibility coefficient	Max. value (%)
As-cast	Shrinkage void, only	–0.361	203.8	–2.219	5.08
	Mixed (shrinkage + bifilm)	–1.106	229.8	–3.441	4.23
	Oxide bifilms, only	–3.575	246.4	–11.344	5.10
T6-treated	Shrinkage void, only	–0.279	332.6	–2.348	1.90
	Mixed (shrinkage + bifilm)	–0.554	343.4	–2.878	1.55
	Oxide bifilms, only	–1.518	337.0	–7.752	1.38

As summarized in Table 4, the defect susceptibility coefficients for specimens containing oxide bifilms are significantly higher than those for specimens containing only shrinkage voids. When considering only oxide bifilms as the overall casting defect, the defect susceptibility coefficients for tensile strength and elongation under the as-cast condition are 3.575 and 11.344, respectively, compared to 0.361 and 2.219 for specimens with only shrinkage voids. For the T6-treated condition, similar trends are observed, with defect susceptibility coefficients of 1.518 and 7.752 for specimens

with only oxide bifilms, versus 0.279 and 2.348 for specimens with only shrinkage voids. Thus, the defect susceptibility coefficient of T6-treated condition shows a lower value than that of the as-cast condition. This is because the plastic deformation behavior of the matrix region adjacent to the casting defect is suppressed due to the strengthening effect of the pro-eutectic Al matrix region generated during the T6 treatment process, thereby delaying the growth of the tensile crack derived from the casting defect. In addition, it should be noted that the maximum tensile properties achievable under defect-free conditions differ from the variation in defect susceptibility coefficients at a given area fraction of casting defects.

Figure 9 schematically illustrates the relative contributions of each type of casting defect to the defect susceptibility of tensile strength and elongation for the T6-treated condition, as summarized in Figure 8. In Figure 9, $\Delta S/\Delta f$ and $\Delta e/\Delta f$ represent the overall sensitivity of tensile strength and elongation to changes in the area fraction of casting defects, corresponding to the defect susceptibility coefficients *b* and *a* in Eqs 1 and 2, respectively. As shown, the defect susceptibility coefficients gradually increase when oxide bifilms are introduced in addition to shrinkage voids. From this, it can be seen that under conditions where micro-voids and oxide bifilms exist at the same area fraction, the effect of oxide bifilms on the defect susceptibility of tensile properties increases more significantly than that of micro-voids.

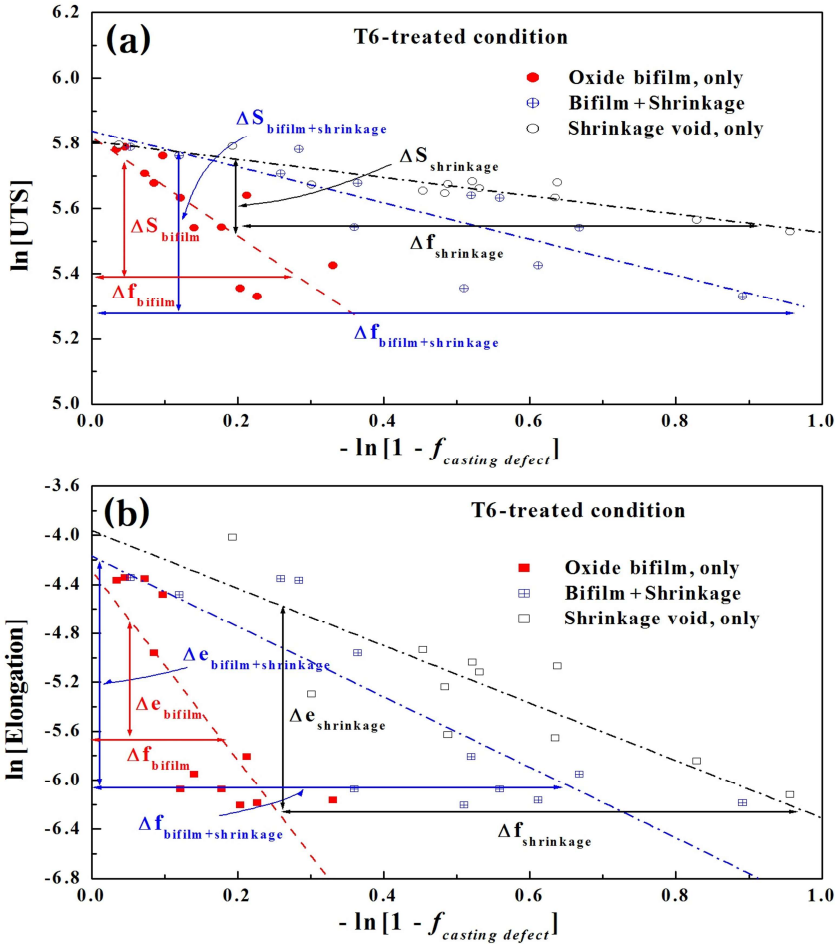

Figure 9. Schematic representation of the relative contributions of shrinkage voids and oxide bifilms to the defect susceptibility of tensile properties under T6 treatment conditions: (a) ultimate tensile strength, (b) elongation.

5. Conclusions

1. The yield strength of A356 alloys produced via gravity casting shows little dependence on the area fraction of casting defects, including shrinkage voids and oxide bifilms. In contrast, ultimate tensile strength and elongation decrease markedly with increasing defect fraction. In the as-cast condition, as the area fraction of defects rises to 0.6, ultimate tensile strength and elongation decrease from ~200 MPa and 4.8% to 150 MPa and 0.6%, respectively. Under T6 treatment, similar trends are observed, with ultimate tensile strength and elongation decreasing from ~330 MPa and 2.0% to 250 MPa and 0.25%.

2. The average area fraction of oxide bifilms on the fracture surface is 12.5%, lower than the total defect area fraction of 32.9%. The inclusion frequency of oxide bifilms was 44.9%, which was lower than the micro-voids observed in all tensile test specimens produced in this study.

3. The presence of micro-voids and oxide bifilms fundamentally influences the tensile properties, but oxide bifilms have a relatively easier tendency to shorten the fracture path through interfacial separation compared to micro-voids. Therefore, the tensile properties of specimens containing both micro-voids and oxide bifilms are more sensitive to changes in the area fraction of casting defects than those containing only micro-voids. In any case, through the T6 treatment, the defect susceptibility coefficients for tensile strength and elongation were clearly improved compared to the as-cast condition.

4. Considering only oxide bifilms as the casting defect, the defect susceptibility coefficients for tensile strength and elongation in the as-cast condition are 3.575 and 11.344, respectively—approximately 9.9 and 5.1 times higher than those for specimens containing only shrinkage voids (0.360 and 2.219). Under T6 treatment, similar trends are observed, with values of 1.518 and 7.752 compared to 0.279 and 2.348 for shrinkage void-only specimens.

Use of AI tools declaration

The author declares that no artificial intelligence (AI) tools were used in the creation of this article.

Acknowledgements

This research was supported by the Development Program for Automotive Industrial Technology through the Korea Evaluation Institute of Industrial Technology (KEIT), funded by the Ministry of Trade, Industry and Energy (RS-2024-00410275). Additional support was provided by the Promotion Business Program of the Advanced Technology Center through KEIT, also funded by the Ministry of Trade, Industry and Energy (20023321).

Conflict of interest

The author declares no conflict of interest.

References

1. Campbell J (2011) *Complete Casting Handbook: Metal Casting Processes, Metallurgy, Techniques and Design*, Boston: Butterworth-Heinemann.

2. Eisaabadi BG, Davami P, Kim SK, et al. (2012) Effects of hydrogen and oxides on tensile properties of Al-Si-Mg cast alloys. *Mater Sci Eng A* 552: 36–47. https://dx.doi.org/10.1016/j.msea.2012.04.111
3. Eisaabadi BG, Varahram N, Davami P, et al. (2012) Effect of oxide bifilms on the mechanical properties of cast Al-7Si-0.3Mg alloy and the roll of runner height after filter on their formation. *Mater Sci Eng A* 548: 99–105. https://doi.org/10.1016/j.msea.2012.03.097
4. Dispinar D, Akhtar S, Nordmark A, et al. (2010) Degassing, hydrogen and porosity phenomena in A356. *Mater Sci Eng A* 527: 3719–3725. https://doi.org/10.1016/j.msea.2010.01.088
5. Dispinar D, Campbell J (2011) Porosity, hydrogen and bifilm content in Al alloy castings. *Mater Sci Eng A* 528: 3860–3865. https://doi.org/10.1016/j.msea.2011.01.084
6. Bogdanoff T, Borjesson J, Seifeddine S, et al. (2023) On the secondary cracks during crack propagation in an Al-Si-Cu-Mg alloy: An in-situ study. *Mater Charact* 203: 113046. https://doi.org/10.1016/j.matchar.2023.113046
7. Eisaabadi BG, Tiryakioğlu M, Davami P, et al. (2014) The effect of remelting on the melt and casting quality in Al–7%Si–Mg castings. *Mater Sci Eng A* 605: 203–209. https://doi.org/10.1016/j.msea.2014.03.032
8. Tiryakioğlu M, Yousefian P, Eason PD (2018) Quantification of entrainment damage in A356 aluminum alloy castings. *Metall Mater Trans A* 49: 5815–5822. https://doi.org/10.1007/s11661-018-4865-z
9. Bogdanoff T, Tiryakioğlu M, Jarfors AEW, et al. (2023) On the combined effects of surface quality and pore size on the fatigue life of Al-7Si-3Cu-Mg alloy casting. *Mater Sci Eng A* 885: 145618. https://doi.org/10.1016/j.msea.2023.145618
10. Song H, Zhang L, Cao F, et al. (2021) Three-dimensional reconstruction of bifilm defects. *Scr Mater* 191: 179–184. https://doi.org/10.1016/j.scriptamat.2020.09.040
11. Sahin H, Dispinar D (2025) Estimating toughness limit of cast aluminum alloys with reduced pressure test. *Inter Metalcast* 19: 2161–2167. https://doi.org/10.1007/s40962-024-01453-y
12. Kutsal U, Colak M, Ertugrul O (2025) Relationship between aluminum liquid metal quality and defects. *Inter Metalcast* https://doi.org/10.1007/s40962-025-01733-1
13. Liu J, Wang Q, Qi Y (2019) Atomic simulation of the formation and fracture of oxide bifilms in cast aluminum. *Acta Mater* 164: 673–682. https://doi.org/10.1016/j.actamat.2018.11.008
14. Kavousi S, Zaeem MS (2023) Mechanisms of nucleation and defect growth in undercooled melt containing oxide clusters. *Acta Mater* 252: 118942. https://doi.org/10.1016/j.actamat.2023.118942
15. Gokhale AM, Patel GR (2005) Origins of variability in the fracture-related mechanical properties of a tilt-pour-permanent-mold cast Al-alloy. *Scr Mater* 52: 237–241. https://doi.org/10.1016/j.scriptamat.2004.09.011
16. Gokhale AM, Patel GR (2005) Quantitative fractographic analysis of variability in tensile ductility of a squeeze cast Al-Si-Mg base alloy. *Mater Character* 54: 13–20. https://doi.org/10.1016/j.matchar.2004.10.003
17. Lee CD, Shin KS, Kim YJ (2017) Dependence of tensile ductility on damage evolution of eutectic Si-particles and pre-existing micro-voids in Al-Si casting alloy. *Eng Mater Frac* 175: 339–356. https://doi.org/10.1016/j.engfracmech.2016.12.014

18. Lee CD, Shin KS (2014) Constitutive prediction of the defect susceptibility of tensile properties to microporosity variation in A356 aluminum alloy. *Mater Sci Eng A* 599: 223–232. https://doi.org/10.1016/j.msea.2014.01.091
19. Lee CD (2018) Effect of artificial ageing on the defect susceptibility of tensile properties to porosity variation in A356 aluminium alloys *Inter Metalcast* 12: 321–330. https://doi.org/10.1007/s40962-017-0168-1
20. Uludağ M, Gurtaran M, Dispinar D (2020) The effect of bifilm and Sr modification on the mechanical properties of AlSi12Fe alloy. *Arc Found Eng* 20: 99–104. https://doi.org/10.24425/afe.2020.133337
21. El-Sayed MA, Essa K, Hassanin H (2022) Effect of runner thickness and hydrogen content on the mechanical properties of A356 alloy castings. *Inter Metalcast* 16: 2175–2186. https://doi.org/10.1007/s40962-021-00753-x
22. Liu L, Zhou W, Liu F, et al. (2024) Melt quality of A356.2 alloy in the pressure counter pressure casting process for steering knuckles. *Inter Metalcast* 18: 1247–1261. https://doi.org/10.1007/s40962-023-01079-6

AIMS Press